Volume 24 (1) 2025

Page 61 - 72

Mekanika: Majalah Ilmiah Mekanika

Numerical Analysis of Six Degrees of Freedom Motion Response of Trimaran Semi-Submersible Ship

Musdika Bagas Satria Putrananda[1], Aldias Bahatmaka[1*], Widya Aryadi[1], Berliana Ayarent Puteri[1], Christian Imanuel Hutagalung[1]

1 Department of Mechanical Engineering, Universitas Negeri Semarang, Semarang, Indonesia

*Corresponding Author's email address: aldiasbahatmaka@mail.unnes.ac.id

Keywords:
Trimaran Ship
Response Amplitude Operator
Six Degree of Freedom
Motion Response
ANSYS AQWA

Abstract
This study examines the motion response characteristics of a trimaran semi-submersible vessel, with a focus on its performance in tourism applications where passenger comfort is a primary concern. Using ANSYS AQWA simulation software, this analysis integrates diffraction and radiation theory with potential flow theory to evaluate the six degrees of freedom (surge, sway, heave, roll, pitch, and yaw) under various wave conditions, including different frequencies and directions based on the Joint North Sea Wave Project (JONSWAP) spectrum. Simulations were performed on waves with heading angles ranging from 0° to 180°. The simulation results were validated based on previous studies both experimentally and numerically. The results show that the sway peaks at 8 m/m for heading angles of 90°, while the surge reaches a maximum of 8 m/m at 0° and 180°. The heave motion resonates between 2.2 rad/s with a peak amplitude of 3 m/m at 90°. Pitch motion at heading angles of 0° reaches 40 °/m at 3.5-4 rad/s. Roll motion remained within acceptable limits (9 °/m), and yaw peaked at 13 °/m at 45° and 135°. These findings suggest that, although the trimaran exhibits stable performance in most motion responses, design improvements are necessary to mitigate excessive pitch motion and enhance passenger comfort in tourism applications.

1 Introduction

Trimaran ships have garnered significant attention in maritime research in recent years due to their superior potential in various applications [1,2]. A trimaran comprises a central main hull flanked by two smaller side hulls. A design that enhances stability, wave resistance, maneuverability, and hydrodynamic performance [3-5]. The ship's design also allows it to penetrate or cut through waves rather than simply passing through them, thereby reducing the impact of waves on the ship's movement and improving operational comfort [6]. These attributes make trimarans ideal for modern maritime operations. The study of ship motion, particularly in terms of hydrodynamic performance, is crucial for optimizing vessel design. Ship motion dynamics in marine environments encompass Six Degrees of Freedom (6-DOF), which can be categorized into two fundamental types: translational motion, which involves linear movement along the x, y, and z axes, and rotational motion, which describes angular movement around the ship's axis [7].

https://dx.doi.org/10.20961/mekanika.v24i1.99057

Revised 17 March 2025; received in revised version 20 March 2025; Accepted 21 March 2025
Available Online 31 March 2025

2579-3144

Understanding these motions is essential for refining the design of semi-submersible trimarans, as they reflect the complex interplay between the ship's structure and hydrodynamic forces [1]. Previous research has made substantial contributions to understanding ship motion responses. For instance, studies employing the Rankine Panel Method have analyzed the time-domain motion and incremental resistance of trimarans in waves, highlighting multi-hull configurations' inherent stability and resistance advantages [8]. Computational Fluid Dynamics (CFD) methods have also examined hull shape effects on stability and deck wetness probability [9]. Experimental and CFD analyses of catamarans have also focused on wave interactions and stability under varying conditions [10]. Numerical studies using ANSYS AQWA have further explored the influence of buoy skirt geometry on motion response and Wave Current Interactions (WCI) [11]. In addition, Experimental and CFD simulations of sandglass-type Floating Production Storage and Offloading (FPSO) have demonstrated how specific hull structures can mitigate slamming intensity through heave and pitch motions [12].

Despite these advancements, a gap remains in numerical studies focusing on the wave response of multi-hull vessels, particularly semi-submersible trimarans, in marine tourism applications. Limited research has been conducted on the Response Amplitude Operator (RAO) characteristics of these vessels under various wave conditions and heading angles, particularly in calm waters. This study addresses this gap by investigating the 6-DOF motion characteristics of a semi-submersible trimaran using ANSYS AQWA. The software was chosen for its robust capabilities in implementing diffraction and radiation theory integrated with potential flow theory, making it highly effective for analyzing wave-induced motions in marine structures [13]. The numerical approach offers significant advantages in terms of time, cost, and resource efficiency compared to traditional experimental methods while still providing accurate and comprehensive RAO data.

This study aims to show that the trimaran semi-submersible exhibits a stable motion response in degrees of freedom under various wave conditions. However, excessive RAO motions may occur at certain bow angles, so it is necessary to conduct further research and design modifications to improve passenger comfort. These findings are expected to significantly contribute to the design and optimization of trimaran vessels for marine tourism. Nevertheless, further experimental research will be required to strengthen and validate the numerical results and ensure their reliability.

2 Numerical Methods

2.1 Theory Framework

2.1.1 Diffraction and Radiation Theory

ANSYS AQWA implements frequency-domain and time-domain analysis methodologies that are essential in investigating the dynamic behavior of marine structures under wave loading. The software applies the boundary element method based on the velocity potential equation referred to in Equation 1 to solve wave-structure interaction problems, enabling high-accuracy modeling of the marine environment [7]. To solve these equations numerically, the panel method is used to discretize the wetted surface of the structure.

Panel diffraction and radiation theory integrated with potential flow theory is a practical approach to analyzing the interaction between waves and floating objects. In this context, potential flow theory focuses on nonviscous and irrotational fluid flow, where the velocity potential can be defined. When analyzing the interaction of floating objects with waves, two primary phenomena occur: diffraction and radiation. As illustrated in Equations 1-3 [14], diffraction refers to the change in the direction of a wave caused by the presence of an object, while radiation pertains to the waves produced by the object's motion [15].

$$\begin{cases} \nabla^2\varphi = 0 \\ \frac{\partial^2\varphi}{\partial t^2} + g\frac{\partial\varphi}{\partial z} = 0 \\ \frac{\partial\varphi}{\partial n} = v(t)n_j \\ \partial\varphi/\partial z = 0 \end{cases} \quad (1)$$

The diffraction equation can be defined:

$$\phi_D^I(\mathrm{r},\theta,\mathrm{z}) = \phi_I^I(\mathrm{r},\theta,\mathrm{z}) + \phi_P^I(\mathrm{r},\theta,\mathrm{z}) \quad (2)$$

The radiation equation can be defined:

$$\phi_R(\mathrm{r},\theta,\mathrm{z}) = \sum_{j=1,3,5} -i\omega\xi_j\phi_j(r,z)\cos m\theta \quad (3)$$

2.1.2 Response Amplitude Operator (RAO)

Response Amplitude Operator (RAO) is a measure that describes the characteristics of a ship's response to regular waves [16,17]. RAO is used to analyze the ship's response to each Degree of Freedom (DOF) based on the wave frequency, as seen in Figure 1. This parameter predicts how the vessel responds to various types of wave-induced motions, such as surge, rocking, and heaving, making it a key element in the analysis of ship stability and performance in the marine environment [7]. Validation of RAO calculations can be done through experimental or numerical methods, such as using ANSYS AQWA software. This approach ensures high accuracy in the design and evaluation of ship performance while increasing the reliability of ship behavior analysis under various dynamic wave conditions [10]. The analysis results are displayed as Response Amplitude Operators (RAOs), which show the ratio of the structure & response to the wave amplitude at various frequencies [18].

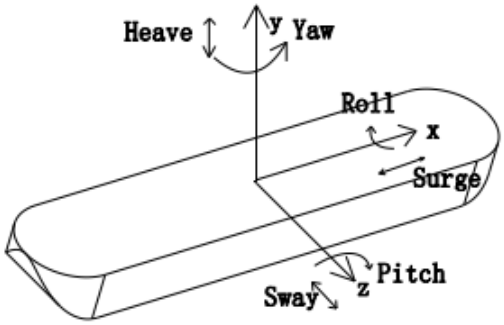

Figure 1. Degree of freedom schematic [7]

2.1.3 JONSWAP Spectrum Analysis

The JONSWAP spectrum is a wave spectrum model derived from observations in the North Sea. This model has the advantage of representing waves in the early stages of development, particularly under the influence of wind. In ANSYS AQWA simulations, the JONSWAP spectrum is used to simulate random wave conditions and analyze the hydrodynamic response of offshore structures, including the movement of six degrees of freedom and the interaction of wave forces with the structure. The JONSWAP spectrum is defined by the following Equation 4 [19]:

$$S\zeta(\omega) = \alpha g^2\omega^{-5}\exp\{-1.25(\omega/\omega_0)^{-4}\}\gamma^{\exp\left\{-\frac{(\omega-\omega_0)}{2\tau\omega_0^2}\right\}} \quad (4)$$

Figure 2 shows a comparison of the JONSWAP spectrum with other wave spectra. The wave standard referred to in [20,21], compares the JONSWAP spectrum and the Pierson-Moskowitz (PM) spectrum, two commonly used spectrum models in marine wave analysis. The JONSWAP spectrum was developed based on measurement data from the North Sea, and the PM spectrum was modified by adding a peakedness parameter.

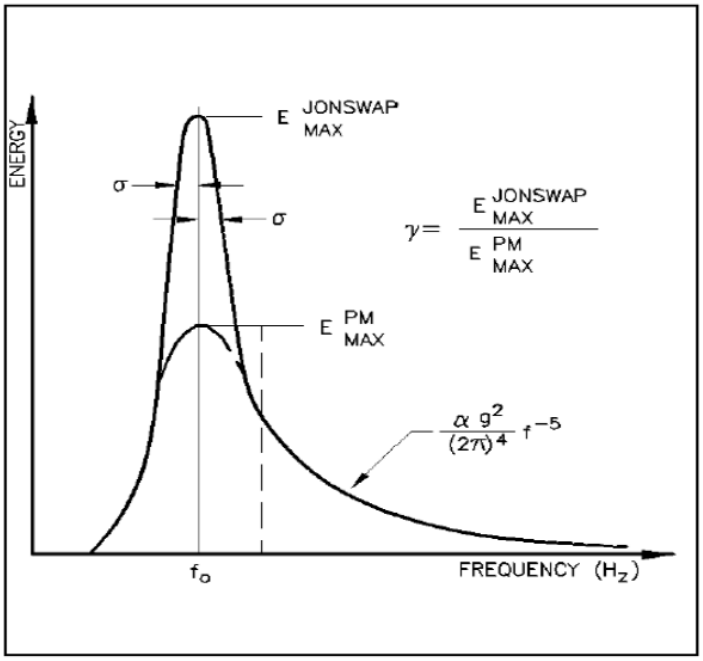

Figure 2. JONSWAP wave spectrum [21]

2.2 Numerical Setup

2.2.1 Trimaran Semi-Submersible Geometry

The trimaran ship model for the ANSYS AQWA simulation was developed using a two-step software process to ensure geometric accuracy and hydrodynamic compatibility. Initially, the model was designed using CAD software, which was chosen for its advanced 3D modeling capabilities and support for iterative design adjustments. Upon completion, the model was exported to ANSYS SpaceClaim using compatible file formats (STEP or IGES) to maintain geometric integrity. In SpaceClaim, the model is optimized for hydrodynamic analysis by removing non-essential details and ensuring closed surfaces are free of errors, such as gaps or intersections, which are critical for accurate panel discretization in ANSYS AQWA. This simplified process yielded a precise trimaran model suitable for simulating hydrodynamic responses in various maritime conditions, thereby ensuring that the simulation accurately reflected the vessel's geometry. The final model specifications are detailed in Table 1 and Figure 3.

Table 1. Trimaran semi-submersible dimensions

Description	Dimension	Unit
Overall length (LOA) – upper section	8.5	m
Overall length (LOA) – lower section	7.0	m
Beam of main hull (upper section)	2.4	m
Beam of main hull (lower section)	1.8	m
Overall beam (including side hulls)	4.6	m
Draft of the main hull	1.695	m
Freeboard height of the main hull	1.1	m
Distance between side hulls and main hull	0.5	m
Beam of each side hull	0.6	m

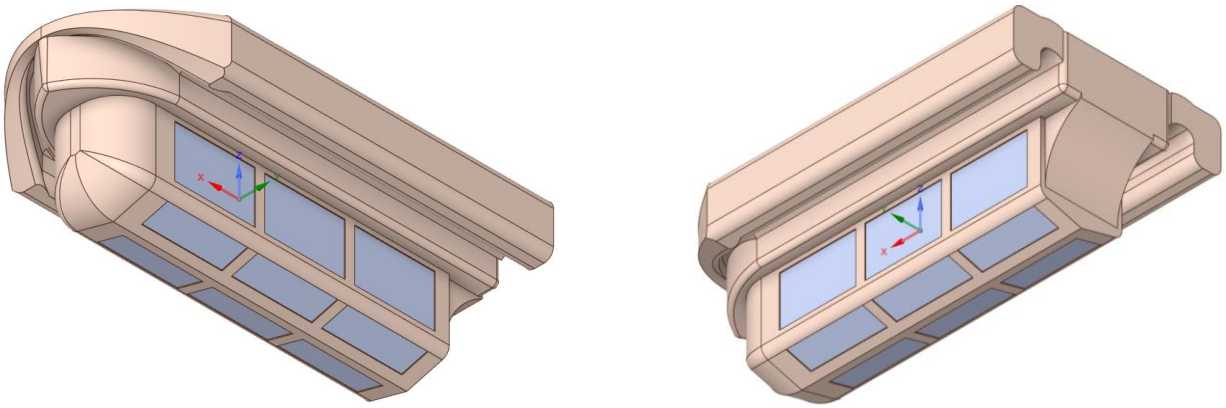

Figure 3. Semi-submersible trimaran ship geometry

2.2.2 Boundary Condition

The boundary condition is crucial in hydrodynamic analysis to define fluid-structure-environment interactions, encompassing fluid flow continuity, energy equilibrium, and seabed interactions [10]. The ship is positioned at the center of the boundary condition, as detailed in Table 2.

Table 2. Boundary condition setup

Description	Value	Unit
Water depth	15	m
Water surface area (*X*)	36	m
Water surface area (*Y*)	50	m
Water density	1025	kg/m³
Gravity	9.8	m/s²

A point mass represents a concentrated mass at a specific location, simulating the weight distribution of non-structural components (e.g., cargo or equipment) without requiring detailed geometry. Suppose a Program Controlled point mass is used. In that case, the mass and the horizontal position will be calculated from the panel elements in the structure (i.e., excluding tubular stub lines and point buoyancy bodies). The mass will equal the mass of water displaced, and the horizontal position will be the center of buoyancy [22]. Key parameters include mass value, location, and moment of inertia. Table 3 presents the specifications for the point mass of the trimaran vessel in this study.

Table 3. Point mass of trimaran semi-submersible ship

Description	Value	Unit
X	-0.143693035339025	m
Y	-1.68660799286878	m
Z	0	m

Inertia properties describe the mass distribution and moment of inertia about the structure's rotational axes [23], which are crucial for evaluating dynamic responses to external forces, such as waves or currents. These properties are defined in global or local coordinates, with the formulas in Equations 5-7 [24]. Table 4 summarizes the inertial properties based on the dimensions of the trimaran vessel used in the simulation.

$$k_{xx} = 0.34 \times \text{Beam} \quad (5)$$

$$k_{yy} = 0.25 \times \text{Length} \quad (6)$$

$$k_{zz} = 0.26 \times \text{Length} \quad (7)$$

Table 4. Inertia properties of trimaran semi-submersible ship

Description	Value	Unit
k_{xx}	0.816	m
k_{yy}	2.125	m
k_{zz}	2.21	m

Wave setup determines the characteristics of ocean waves, including wave type (regular or irregular), height, period, and direction. Regular waves are used for simplified analysis, while irregular waves (imbalance of energy flow), modeled using energy spectra such as JONSWAP, represent complex ocean conditions [22]. These settings ensure realistic simulations in various environmental scenarios. Table 5 outlines the wave settings applied in this study, based on Equation 4, which is derived from the JONSWAP spectrum and its associated spectrum pattern, as shown in Figure 2.

Table 5. Wave condition setting

Description	Value
Wave type	JONSWAP
Wave range	0°-180°
Speed	2 m/s
Initial condition	180°
Start frequency	0.1 rad/s
Finish frequency	5.26 rad/s
Interval	45°
Wave amplitude	0.2 m

2.2.3 Mesh Setting

In this study, the mesh is crucial for ensuring the accuracy of hydrodynamic simulations. It is generated using the panel discretization method, which divides the wetted surface into panels that represent sources and dipoles for fluid-structure interaction calculations. Detailed specifications are provided in Table 6. Table 7 presents the results derived from the analysis of mesh skewness conducted in this study.

Table 6. Mesh setting

Description	Value	Unit
Element size	0.3	m
Connection tolerance	0.03	m
Maximum allowed frequently	5.26	rad/s
Total nodes	1685	-
Total element	1685	-

Table 7. Mesh skewness

Mesh	Element	Size (m)	Average Skewness	Element Skewness < 0.25
Coarse	889	0.5	0.25	65.5%
Medium	1041	0.4	0.21	76.8%
Fine	1685	0.3	0.19	78%

2.2.4 Validation and Convergence of the Simulation Method

The validation and convergence of the simulation method are crucial steps to ensure the reliability, accuracy, and robustness of the numerical results. This section comprehensively addresses the mesh quality assessment, convergence analysis, and validation of the method's accuracy against experimental or benchmark data. Mesh quality has a significant impact on numerical accuracy and stability. A well-constructed mesh reduces discretization errors and enhances convergence. This study assessed mesh quality using skewness. Three configurations, coarse, medium, and fine, were tested to optimize computational efficiency and accuracy.

Convergence analysis assesses the stability and consistency of the solution under mesh smoothing. Simulations were conducted with coarse, medium, and fine meshes, monitoring the Six Degrees of Freedom (6-DOF) response over time. Figure 4 illustrates the trend of the wave frequency response as a function of time. The results show that the solution converges asymptotically, confirming mesh independence. As in Table 6, the fine mesh was chosen for optimal accuracy and computational cost balance.

To validate the accuracy of the simulation method, the numerical results are compared with experimental data or numerical analytical solutions of reference cases. The comparison is focused on the main output parameters. In this study, one parameter, i.e., roll, is taken. The validation results are presented in Figure 5 and Table 8, which show a good agreement between the numerical and experimental data, with an average relative error of 5.6% compared to the experimental results and 4.21% compared to the study, as reported by Chen et al. [25]. This confirms the accuracy and reliability of the simulation method.

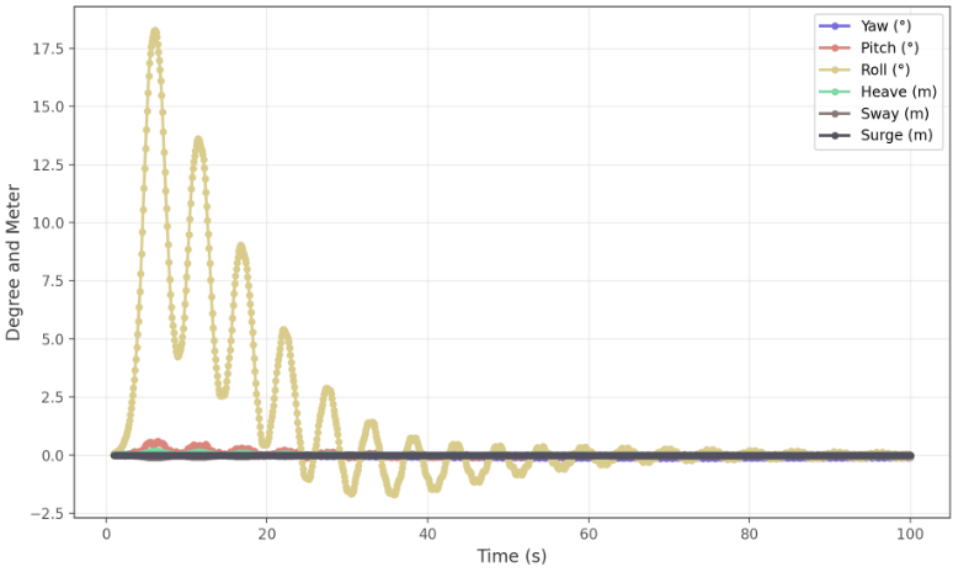

Figure 4. Convergence of wave frequency response results from 1 to 100 seconds

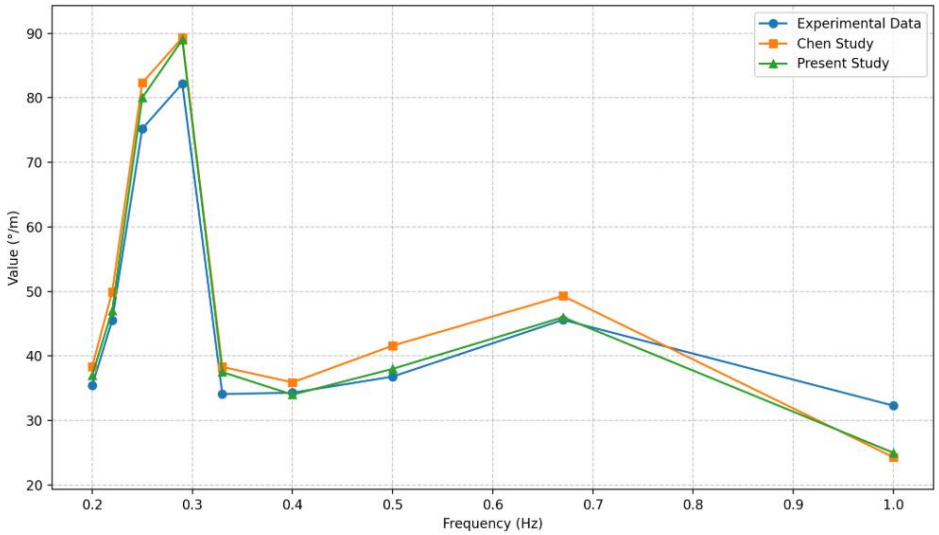

Figure 5. Comparison of RAO in roll versus wave frequency in the current method with previous research (Chen et al. [25])

Table 8. A comparison of RAO variations in roll versus wave frequency was made in the present study and previous research

Frequency (Hz)	Experimental Data (°/m)	Present Study (°/m)	Difference (%)
0.2	35.4	37.2	5.08
0.22	45.5	47.5	4.40
0.25	75.2	80	6.38
0.29	82.2	88.9	8.15
0.33	34.1	37	8.50
0.4	34.3	34.1	0.58
0.5	36.8	38.2	3.80
0.67	45.6	46.9	2.85
1	32.3	26.1	19.20

After validating the method using experimental data and numerical results from previous studies, a consistent trend was observed between the two. The resulting error values are consistently below 10%, indicating high accuracy. This confirms the validity of the method used in Response Amplitude Operator (RAO) simulations in this study, making it reliable for further analysis.

2.3 Flowchart Numerical Method

Figure 6 illustrates a summary of the simulation workflow. The process begins with the creation of geometry using Autodesk Inventor and ANSYS SpaceClaim, followed by domain setup to define the boundaries. A mesh quality check ensures its accuracy. If (yes) it meets the standards, the process proceeds to waveform setup; if (no), adjustments to the geometry are required. Solution setup determines the numerical parameters, and solution convergence assesses the stability of the results. If convergence is achieved, the analysis will proceed to the result stage; otherwise, further adjustments are required.

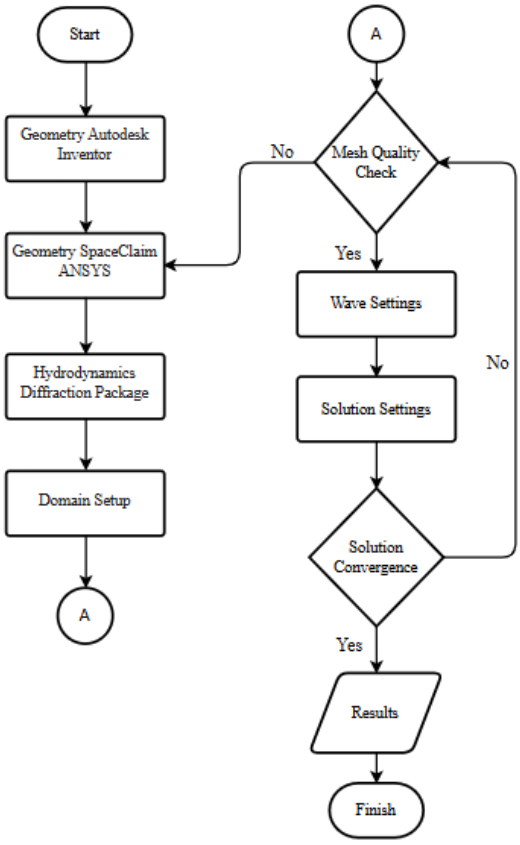

Figure 6. Numerical simulation flowchart

3 Results and Discussion

3.1 RAO Simulation Results Based on Frequency Domain

In this study, frequency domain hydrodynamic analysis was performed using ANSYS AQWA software. Diffraction and radiation methods were used to consider the angle between the heading angle and the wave direction. The six wave directions that were the focus of the study include: head sea (180°), bow sea (135°), beam sea (90°), quartering sea (45°), and following sea (0°). This study employs an innovative model of a trimaran semi-submersible vessel, specifically designed for marine operations. The simulated wave conditions correspond to calm water conditions, as listed in Table 5. The numerical analysis results obtained, particularly the Response Amplitude Operator (RAO), are shown in Figure 7.

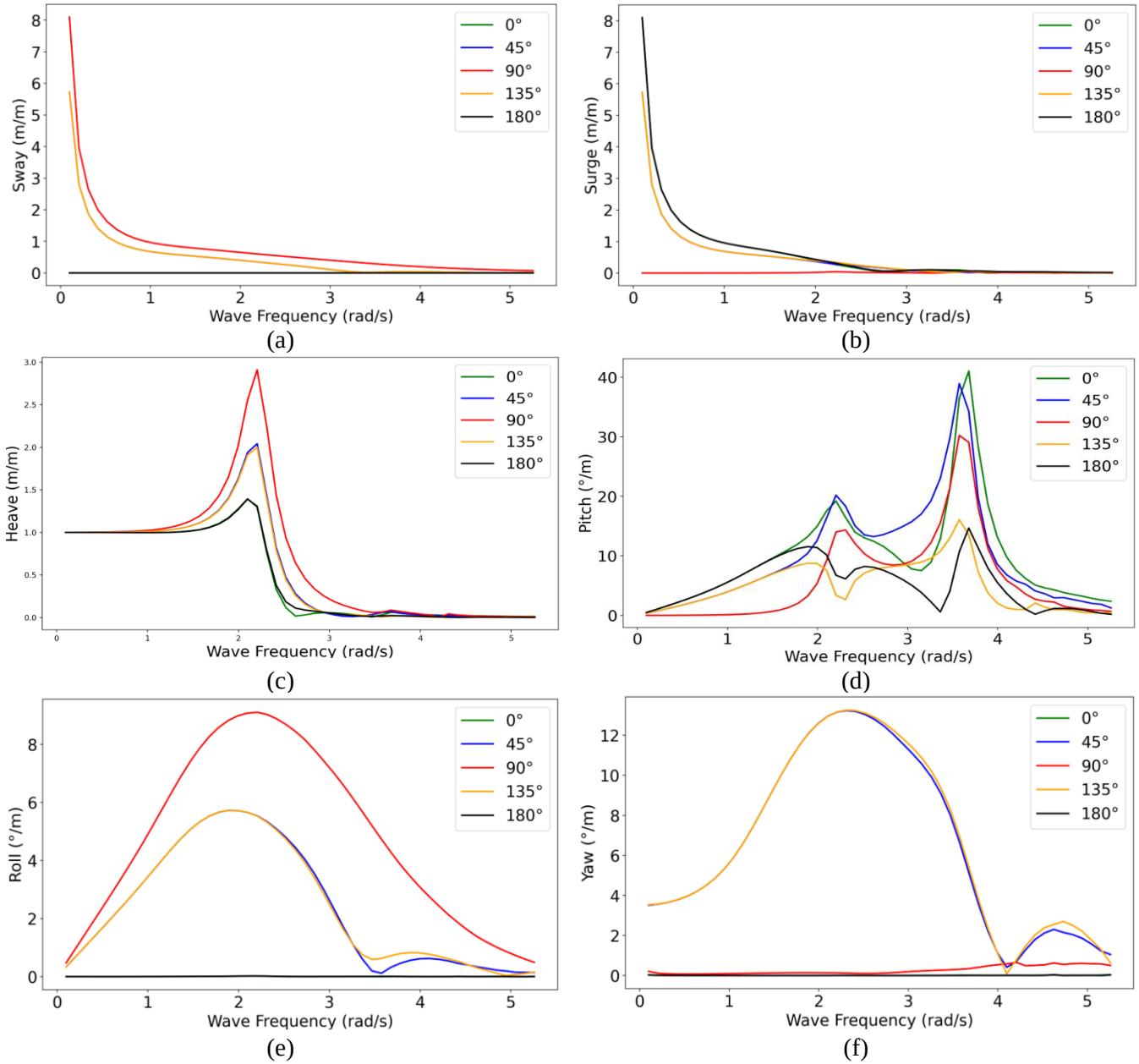

Figure 7. Six RAO of the trimaran semi-submersible ship, in this case: (a) Sway; (b) Surge; (c) Heave; (d) Pitch; (e) Roll; and (f) Yaw

The sway RAO of the trimaran semi-submersible vessel is presented in Figure 7 (a). As Figure 7(a) shows, it reaches its highest values at low frequencies (<1 rad/s), especially at 90° angles, indicating a maximum lateral response due to waves from the hull side. However, the sway RAO decreases dramatically at frequencies greater than 1 rad/s, indicating a low response to high-frequency waves. At angles of 0° and 180°, the sway RAO is minimal due to waves coming from the front and rear, which reduces the lateral force. Diagonal angles (45° and 135°) show intermediate sway RAO values, with wave components partially contributing to the lateral motion.

The surge RAO is shown in Figure 7 (b). The peak value is similar to sway, the difference being the angle of the RAO. Wave At an angle of 0° and 180°, the ship moves translational against the wave direction. The wave RAO reaches the highest value at low frequencies (0-0.5 rad/s), indicating a high response to long waves. However, the RAO decreases significantly at frequencies greater than 1 rad/s, indicating a low response to short waves. 90° angles have the lowest RAO due to lateral motion or sway dominance. Angles of 45° and 135° show intermediate RAO values, reflecting the influence of wave components contributing to the waves.

As shown in Figure 7 (c), at low frequencies (<2 rad/s), the heave RAO is relatively constant at all angles, indicating a uniform response to long waves. The resonance peak occurs at 2.2 rad/s, close to the ship's natural frequency in the heave direction, with the highest response at 90° due to the lateral pressure distribution. The 45° and 135° angles show higher heave RAO peaks than the 0° and 180° angles but lower than the 90° angle, as the diagonal wave component still contributes to the vertical motion. The 0° and 180° angles have the lowest heave RAO due to the waves coming from the bow/stern. Above 2.5 rad/s, the heave RAO decreases sharply, indicating minimal response to short waves.

Ship pitch is an oscillatory motion around the transverse axis that causes the bow and stern to rise and fall, influenced by the direction of incoming waves. In Figure 7 (d), the pitch is lower at head sea (180°) due to trimaran wave piercing. The highest peak is 0° because the ship does not break the wave flow. In 135° (forward angle waves), pitch remains with additional rolling due to waves coming from a certain angle. The pitch increases at 45°, and rolling remains, with potential yawing. The Response Amplitude Operator (RAO) shows that the ship's response to waves decreases significantly at higher wave frequencies, possibly due to the ship's natural frequency and stability.

As seen in Figure 7 (e), at angles of 0° and 180°, the roll RAO is close to zero at all frequencies because the wave from the front/rear does not generate enough torsional moment. The resonance peak of the roll occurs at approximately 2.2 rad/s at 90° due to the maximum hydrodynamic moment generated by the lateral force of the wave. Angles of 45° and 135° show lower roll RAOs because the diagonal waves generate partial moments. Above 3 rad/s, the roll RAO decreases sharply due to the dominance of damping and inertia effects, thus reducing the ship's response to high-frequency waves.

Figure 7 (f), also shows similarities with the roll RAO but at different angles. The yaw resonance peak occurs in the 2-3 rad/s range, close to the ship's natural yaw frequency. At an angle of 135°, the oblique incident wave creates an asymmetric lateral force on the hull, thus increasing the yaw motion. Above 3 rad/s, the yaw RAO decreases significantly due to the dominance of damping and inertia effects, reducing the ship's response to high-frequency waves.

3.2 Contour of Trimaran Ship Response to Wave

In addition to the graphical results discussed earlier, this section also displays the wave elevation contours experienced by the ship, as shown in Figure 8. Figure 8 shows the interaction between the ship structure and the waves, where the contours depict the elevation of the wave surface in units of frequency (rad/s). This visualization offers insight into how waves impact the ship. The red contours show the area with the highest wave elevation experienced by the ship, while the blue color shows the lowest wave elevation.

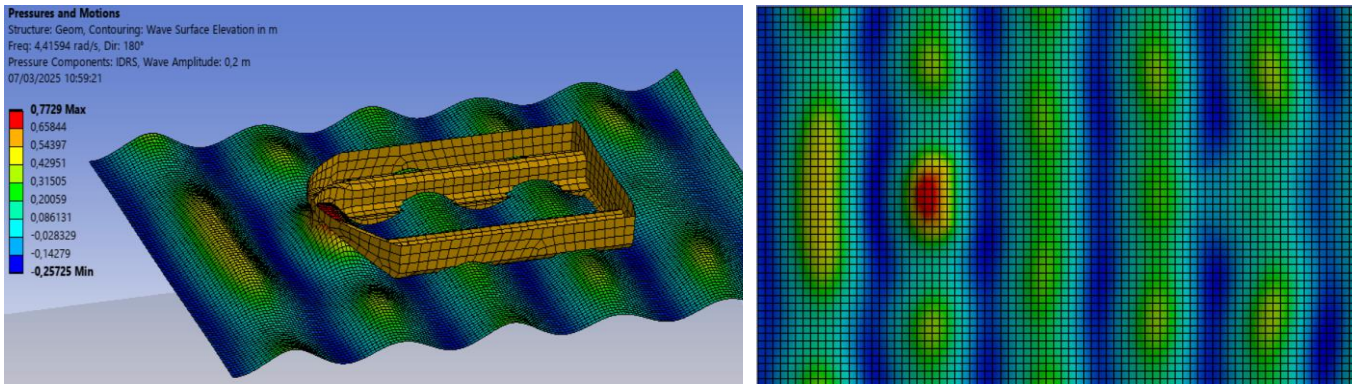

(a) (b)

Figure 8. Contours of wave elevation against ship structure: (a) Interaction of structure with waves; (b) Contour of wave frequency variation

4 Conclusions

This study examines the seakeeping characteristics of a trimaran semi-submersible vessel through RAO analysis. The vessel exhibits quantitatively different hydrodynamic behavior at six degrees of freedom. At low frequencies (<1 rad/s), the vessel exhibited a maximum sway RAO of 8.09 m/m at 0.1 rad/s when encountering a wave angle of 90°. The surge motion reached a peak RAO value of 8.09 m/m at a frequency of 0.1 rad/s for wave angles of 0° and 180°. The heave motion analysis reveals a distinct resonance peak, with the highest RAO of 2.9 m/m at 2.2 rad/s, particularly at a 90° wave angle.

The rotational behavior of the vessel indicates that the pitch response at 180° (head sea) is reduced by 64.39% compared to the following sea (0°), with a minimum RAO of 14.6 deg/m at 3.67 rad/s, which is attributed to the wave-penetrating characteristics of the trimaran design. The roll motion shows obvious resonance at 2.2 rad/s with the RAO reaching 9.1 deg/m at 90° wave angle, while the yaw motion peaks at 13.23 deg/m in the frequency band of 2.3 rad/s at 45° and 135° wave angle. Quantitative analysis confirms that the RAO values decrease by 80% in all motion modes at frequencies above 3 rad/s, except for the pitch motion, which maintains fluctuations. Based on the obtained values, the result remains within the safe limits established by the International Maritime Organization (IMO). These measurable performance characteristics make the trimaran semi-submersible highly suitable for maritime tourism applications.

Acknowledgement

The author would like to thank the Department of Mechanical Engineering at Universitas Negeri Semarang for its support in the research on developing the semi-submersible ship innovation.

References

1. S. Wang, F. Duan, and E. Wang, “Study on the performance and efficiency of multi-objective evolutionary algorithms for trimaran outrigger layout seakeeping optimization problem,” *Ocean Eng.*, vol. 309, article no. 118526, 2024.
2. H. Tang, D. Ren, B. Chen, and C. G. Soares, “A trimaran structure damage identification method based on machine learning,” *Ocean Eng.*, vol. 320, article no. 120315, 2025.
3. M. H. M. Ghazali, M. H. A. Satar, and W. Rahiman, “Unmanned surface vehicles: From a hull design perspective,” *Ocean Eng.*, vol. 312, article no. 118977, 2024.
4. J. Yang, Z. Deng, W. Yu, Z. Zhu, H. Li, and C. Yu, “Research methods for trimaran resistance and optimization analysis of side hull layouts,” *Ocean Eng.*, vol. 320, article no. 120237, 2025.
5. Z. Liu, H. Zhang, L. Shi, K. Shi, G. Chen, and L. Tao, “Numerical and experimental investigation of motion characteristics of a travelling trimaran encountering a freak wave,” *Ocean Eng.*, vol. 317, article no. 120060, 2025.
6. A. A. Khoob, S. M. Pour, and A. Feizi, “Experimental Investigation of a Wave-Piercing Trimaran on the Outrigger Configurations in terms of Seakeeping and Added Resistance,” *J. Appl. Fluid Mech.*, vol. 15, no. 1, pp. 51-62, 2022.

7. H. Xu, P. Neng, and F. Yang, "Motion response analysis of mining vessel based on ANSYS/AQWA," *in the 3rd International Conference on Fluid Mechanics and Industrial Applications*, Taiyun, China, 2019
8. Z. Wu, B. Zhou, Y. Wang, J. Zou, X. Cui, and G. Zhang, "Effects of steady flow and side hull layouts on motions and added resistance of a trimaran sailing in waves," *Ocean Eng.*, vol. 313, article no. 119153, 2024.
9. A. Bahatmaka, D. J. Kim, Samuel, A. Rio Prabowo, and M. T. Zaw, "Investigation on the performance of the traditional Indonesian fishing vessel," *MATEC Web Conf.*, vol. 159, pp. 1-6, 2018.
10. T. L. Mai, A. K. Vo, A. Cho, V. T. Mai, and H. K. Yoon, "Experimental investigation on wave characteristics due to interference of catamaran demi-hulls in waves," *Int. J. Nav. Archit. Ocean Eng.*, vol. 16, article no. 100594, 2024.
11. C. V. Amaechi, F. Wang, and J. Ye, "Numerical studies on CALM buoy motion responses and the effect of buoy geometry cum skirt dimensions with its hydrodynamic waves-current interactions," *Ocean Eng.*, vol. 244, article no. 110378, 2022.
12. T. W. Piao, W. H. Wang, L. J. Wang, C. Geng, K. D. Zhang, and Y. Huang, "Analysis on slamming characteristics of new sandglass-type model in waves with consideration of motion responses," *Ocean Eng.*, vol. 323, article no. 120631, 2025.
13. A. Bahatmaka, A. R. Prabowo, and D. J. Kim, "Effect of Nozzle Performance on the Ducted Propeller: A Benchmark-Simulation Study using OpenFOAM," *Transp. Res. Procedia*, vol. 55, pp. 645-652, 2021.
14. S. Y. Han, B. Bouscasse, V. Leroy, and D. Le Touzé, "Linear diffraction and radiation theory of water waves by a truncated vertical circular cylinder with heave plate in deep and shallow drafts," *Int. J. Nav. Archit. Ocean Eng.*, vol. 16, article no. 100580, 2024.
15. S. Viswanathan, C. Holden, O. Egeland, and M. Greco, "An open-source python-based boundary-element method code for the three-dimensional, zero-froude, infinite-depth, water-wave diffraction-radiation problem," *Model. Identif. Control*, vol. 42, no. 2, pp. 47-81, 2021.
16. N. Dementyev, *Quasi-dynamic global strength analysis of a passenger ship in regular waves*, Espoo: Aalto University, 2019.
17. M. A. Lutfi, A. R. Prabowo, E. M. Muslimy, T. Muttaqie, N. Muhayat, H. Diatmaja, Q. T. Do, S. J. Baek, and A. Bahatmaka, "Leisure Boat Concept Design: Study on the Influence of Hull Form and Dimension to Increase Hydrodynamic Performance," *Int. J. Mech. Eng. Robot. Res.*, vol. 13, no. 1, pp. 139-161, 2024.
18. S. R. Samaei, F. Azarsina, and M. A. Ghahferokhi, "Numerical Simulation of Floating Pontoon Breakwater with ANSYS AQWA Software and Validation of the Results with Laboratory Data," *Bull. la Société R. des Sci. Liège*, vol. 85, pp. 1487-1499, 2016.
19. E. B. Djatmiko, *Perilaku dan Operabilitas Bangunan Laut di Atas Gelombang Acak*, Surabaya: ITS Press, 2012. (*in Indonesian*)
20. K. Hasselmann, T. P. Barnett, E. Bouws, H. Carlson, D. E. Cartwright, K. Eake, J. A. Euring, A. Gicnapp, D. E. Hasselmann, P. Kruseman, A. Meerburg, P. Mullen, D. J. Olbers, K. Richren, W. Sell, and H. Walden, *Measurements of wind-wave growth and swell decay during the joint North Sea wave project (JONSWAP)*, Hamburg: Deutsches Hydrographisches Institut, 1973.
21. H. Veladi and N. Khodadadi, "An experimental study on assessing behavior of quay walls under the action of irregular waves using Artificial Neural Network," *in the 2nd International Congress on science & Engineering*, Paris, France, 2020.
22. Ansys, *AQWA User Manual - Release 14.5*, Pennsylvania: Ansys Inc., 2012.
23. F. I. T. Petrescu, A. Apicella, A. Raffaella, R. V. Petrescu, J. K. Calautit, and A. Riccio, "Something about the mechanical moment of inertia," *Am. J. Appl. Sci.*, vol. 13, no. 11, pp. 1085-1090, 2016.
24. A. Aqwa and H. Diffraction, *Workshop 2.1 14.5*, Pennsylvania: Ansys Inc., 2013.
25. C. W. Chen, Y. Chen, and Q. W. Cai, "Hydrodynamic-interaction analysis of an autonomous underwater hovering vehicle and ship withwave effects," *Symmetry*, vol. 11, no. 10, article no. 1213, 2019.